

A Machine Learning-Based Model for Characterizing Stationary-and-Dynamic Behavior of VCSEL

Original

A Machine Learning-Based Model for Characterizing Stationary-and-Dynamic Behavior of VCSEL / Khan, Ihtesham; Marchisio, Andrea; Tunesi, Lorenzo; Masood, MUHAMMAD UMAR; Ghillino, Enrico; Curri, Vittorio; Carena, Andrea; Bardella, Paolo. - ELETTRONICO. - (2023), pp. 1-2. (CLEO: Science and Innovations San Jose, CA, United States 7-12 May 2023) [10.1364/CLEO_AT.2023.JW2A.141].

Availability:

This version is available at: 11583/2980624 since: 2023-08-23T09:23:32Z

Publisher:

Optica Publ.

Published

DOI:10.1364/CLEO_AT.2023.JW2A.141

Terms of use:

This article is made available under terms and conditions as specified in the corresponding bibliographic description in the repository

Publisher copyright

Optica Publishing Group (formely OSA) postprint/Author's Accepted Manuscript

“© 2023 Optica Publishing Group. One print or electronic copy may be made for personal use only. Systematic reproduction and distribution, duplication of any material in this paper for a fee or for commercial purposes, or modifications of the content of this paper are prohibited.”

(Article begins on next page)

A Machine Learning-Based Model for Characterizing Stationary-and-Dynamic Behavior of VCSEL

Ihtesham Khan⁽¹⁾, Andrea Marchisio⁽¹⁾, Lorenzo Tunesi⁽¹⁾, Muhammad Umar Masood⁽¹⁾, Enrico Ghillino⁽²⁾, Vittorio Curri⁽¹⁾, Andrea Carena⁽¹⁾, Paolo Bardella⁽¹⁾

⁽¹⁾ Politecnico di Torino, Corso Duca degli Abruzzi, 24, 10129, Torino, Italy

⁽²⁾ Synopsys, Inc., 400 Executive Blvd Ste 101, Ossining, NY 10562, United States

paolo.bardella@polito.it

Abstract: We propose a machine learning-based framework to acquire parameters that define stationary-and-dynamic behavior of VCSEL. Circuit-level simulations of light-current and S21 are used to train the model. In terms of relative-prediction-error promising results are achieved. © 2022 The Author(s)

1. Introduction

In recent years, many physical models have been presented to characterize the complex behavior of edge-emitting or vertical-cavity laser diodes. These tools help designers understand laser behavior and maximize device attributes by accurately describing sophisticated physical effects. As a drawback, the number of involved physical parameters (geometrical properties, material characteristics, electrical and thermal effects) can make it challenging to find a correct set of parameters fitting experimental laser measurements, starting with the fundamental Light-Current (L-I) characteristics and the Small Signal Modulation Responses (S21). Extracting physical parameters from experimental curves can be time-consuming, requiring brute-force minimization, trial-and-error tactics, or regression analysis. We present a Machine Learning (ML) approach that can extract from experimental measurements the parameters required by a circuit-level model of a Vertical Cavity Surface Emitting Laser (VCSEL) developed in Synopsys OptSim [1]. We propose a single ML-based agent that can cope with all the electrical, optical, and thermal effects considered in OptSim, unlike prior research that concentrated on edge-emitting devices [2] or required two distinct simulations to account for temperature-dependent effects [3].

2. Vertical Cavity Surface Emitting Laser Model and Dataset Generation

The VCSEL model implemented in OptSim derives from the mean-field model proposed in [4].

The temporal evolution the photon number in the cavity S and their phase ϕ is described as

$$\frac{\partial S}{\partial t} = -\frac{S}{\tau_p} + \frac{\beta_{sp}N_0}{\tau_n} + \frac{G[\gamma_{00}(N_0 - N_t) - \gamma_{01}N_1]}{1 + \varepsilon S} S \quad (1) \quad \frac{\partial \phi}{\partial t} = \frac{\alpha}{2} \frac{G[\gamma_{00}(N_0 - N_{tr}) - \gamma_{01}N_1]}{1 + \varepsilon S} \quad (2)$$

with τ_p photon lifetime and β_{sp} spontaneous emission coefficient, G gain, τ_n carrier lifetime, ε gain saturation factor, α linewidth enhancement factor. The carrier numbers N_0 and N_1 are the result of an expansion in the Bessel series of the total carrier number in cylindrical coordinates [4] $N(r) = N_0 - N_1 J_0(\sigma_1 r/R)$, where the first kind Bessel function $J_0(x)$ is evaluated in the first non-zero root σ_1 of J_1 times the distance r with respect to the VCSEL symmetry axis over the radius of the active layer R . The temporal evolutions of the spatially independent carrier numbers N_0 and N_1 are described as

$$\frac{\partial N_0}{\partial t} = \frac{\eta_i I}{q} - \frac{N_0}{\tau_n} - \frac{G[\gamma_{00}(N_0 - N_t) - \gamma_{01}N_1]}{1 + \varepsilon S} S - \frac{I_1}{q} \quad (3) \quad \frac{\partial N_1}{\partial t} = -\frac{N_1}{\tau_n} (1 + h_{diff}) + \frac{G[\phi_{100}(N_0 - N_t) - \phi_{101}N_1]}{1 + \varepsilon S} S \quad (4)$$

with η_i current injection efficiency, I injected current, q electron charge, N_t carrier transparency number, I_1 leakage current, and h_{diff} diffusion parameter. In 1-4, the terms ϕ_{100} and ϕ_{101} are mode overlap coefficients calculated as functions of the ratio ρ between the characteristic VCSEL radius R_m and R .

The following phenomenological representation of the gain G , the carrier transparency number N_t , and the leakage current I_1 are used to introduce temperature (T) related effects: $N_t(T) = N_{tr} (c_{n0} + c_{n1}T + c_{n2}T^2)$, $G(T) = G_0 \frac{a_{g0} + a_{g1}T + a_{g2}T^2}{b_{g0} + b_{g1}T + b_{g2}T^2}$, $I_1(T) = I_{10} \exp\left(\frac{-a_0 + a_1 N_0 + a_2 N_0 T - a_3 / N_0}{T}\right)$ with I_{10} leakage factor; $a_{g0} - a_{g2}$, $b_{g0} - b_{g2}$, $c_{n0} - c_{n2}$, and $a_0 - a_3$ are fitting coefficients. Finally, the internal temperature of the device is calculated as $T = T_{ref} + (P_{in} - P_{out})R_{th} - \tau_{th} dT/dt$ with T_{ref} 25 °C, P_{in} electrical power entering the device, R_{th} thermal resistance, and τ_{th} thermal time constant.

A dataset of 15000 records is then generated, changing the 24 parameters listed in Table I over to the ranges reported in the same Table. For each combination of these parameters, we store in the dataset points from the L-I curves (at 20 °C, 40 °C, and 60 °C) and from six S21 responses (three at 20 °C, two at 40 °C, and one at 60 °C). Currents range from 0 to 15 mA, frequencies from 100 mHz-50 GHz interval.

Table 1: Parameters investigated and variation ranges for generating dataset.

Parameters	Range	Parameters	Range
Injection efficiency η_i	0.7 to 1	Spont. emission coeff. β_{sp}	0 to 1×10^{-6}
Photons to power k_f	1×10^{-8} W to 6×10^{-8} W	Gain saturation factor ϵ	1×10^{-6} to 5×10^{-6}
Photon lifetime τ_p	1.5 ps to 3.5 ps	Leakage current factor I_{l0}	1 A to 2 A
Carrier lifetime τ_n	0.5 ns to 5 ns	Transp. number param. C_{n0}	1 to 10
Gain coeff. g_0	1×10^4 s $^{-1}$ to 2×10^5 s $^{-1}$	Transp. number param. C_{n1}	-0.1 K $^{-1}$ to -0.01 K $^{-1}$
Gain coeff. a_{g0}	-1×10^4 to -4×10^3	Transp. number param. C_{n2}	0 K $^{-2}$ to 1×10^{-4} K $^{-2}$
Gain coeff. a_{g1}	5 K $^{-1}$ to 20 K $^{-1}$	Leakage current param. a_0	2000 K to 10000 K
Gain coeff. a_{g2}	0.02 K $^{-2}$ to 0.2 K $^{-2}$	Leakage current param. a_1	0 K to 3×10^{-4} K
Gain coeff. b_{g0}	1×10^3 to 1×10^4	Leakage current param. a_2	1×10^{-9} to 4×10^{-8}
Gain coeff. b_{g1}	-100 K $^{-1}$ to 0 K $^{-1}$	Leakage current param. a_3	1×10^8 K to 1×10^9 K
Gain coeff. b_{g2}	0 K $^{-2}$ to 1 K $^{-2}$	Diffusion parameter h_{diff}	1 to 20
Transparency carrier n_{tr}	2×10^6 to 1×10^7	Thermal impedance R_{th}	500 K W $^{-1}$ to 8000 K W $^{-1}$

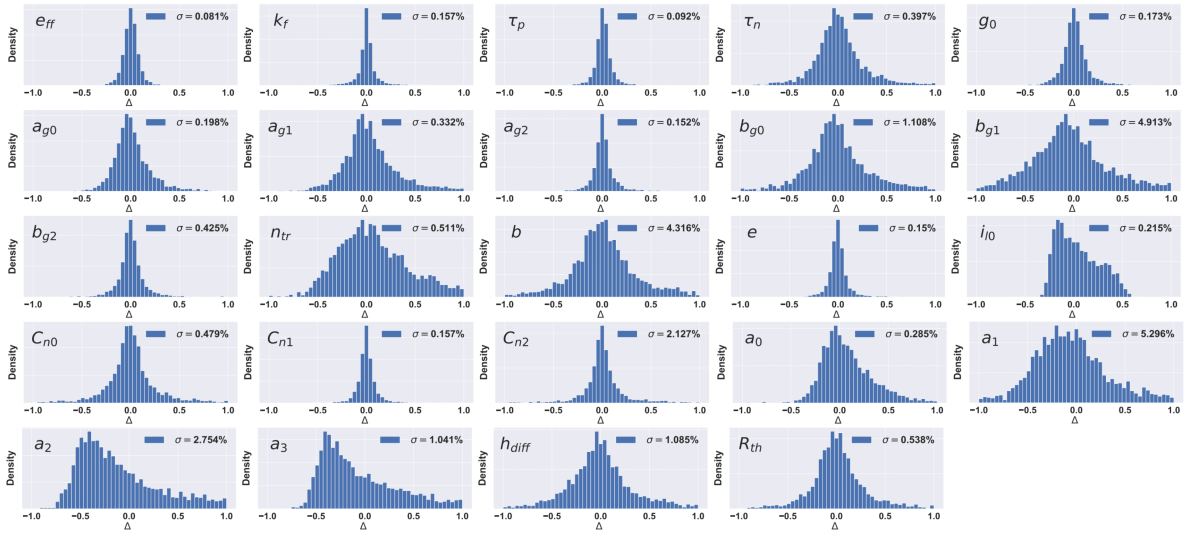


Fig. 1: Relative predicting error and relative error standard deviation of the DNN agent for the 24 parameters.

3. Machine Learning Framework and Results

After retrieving the dataset, we build an ML-based system to extract the 24 VCSEL parameters. The suggested ML agent uses a Deep Neural Network (DNN) with two hidden layers and 20 neurons per layer [5], using 1000 training steps and a 0.001 learning rate. Mean square error is used as the loss function and *ReLU* as the activation function. 70% of the dataset is used for training and 30% for testing. The DNN is built on MATLAB[®] with the DL system Toolbox[™]. A parallel DNN design is suggested to improve prediction accuracy. To extract each distinct VCSEL parameter using parallel DNN, a single DNN unit is proposed. The accuracy of a DNN unit's predictions is measured by the relative prediction error ($\Delta = \frac{\text{Predicted Value} - \text{Actual Value}}{\text{Actual Value}}$) of each parameter. In Fig. 1, the findings of the DL agent are shown as a histogram of the relative error of the investigated parameters and the standard deviation (σ) of the relative-prediction error. The suggested method quickly finds precise VCSEL parameters utilizing an automated and agnostic methodology. Simulations run for a few hours on the latest workstations to build the dataset and DNN agent. The suggested model can be scaled up with excellent accuracy for more parameters due to its parallel design, which can be rapidly enlarged without compromising accuracy. So, the proposed architecture can be used to research different laser classes.

We proposed an ML method to extract physical parameters that characterize the stationary and dynamic behavior of the VCSEL source. Circuit-level simulations of VCSEL L-I and S21 properties, including temperature effects, are considered for generating the datasets. In addition, the suggested technique can easily be adapted to a larger number of parameters in more complex models.

References

- [1] <https://www.synopsys.com/photonic-solutions.html>.
- [2] Z. Ma and Y. Li, "Parameter extraction and inverse design of semiconductor lasers based on the deep learning and particle swarm optimization method," *OE* **28**, 21971–21981 (2020).
- [3] I. Khan *et al.*, "Machine learning-based model for defining circuit-level parameters of vcsel," in *SofCOM*, (2022), pp. 1–6.
- [4] P. Mena *et al.*, "A comprehensive circuit-level model of vertical-cavity surface-emitting lasers," *JLT* **17**, 2612–2632 (1999).
- [5] I. Khan *et al.*, "A neural network-based automatized management of N × N integrated optical switches," in *Photonic Networks and Devices*, (OSA, 2021), pp. NeF2B–2.